Published in final edited form as:
J Am Chem Soc. 2013 April 24; 135(16): 6289–6299. doi:10.1021/ja4014997.

Rational Design of Fatty Acid Amide Hydrolase Inhibitors that Act by Covalently Bonding to Two Active Site Residues

Katerina Otrubova[†,#], **Monica Brown**[§], **Michael S. McCormick**[§], **Gye W. Han**[§], **Scott T. O'Neal**[x], **Benjamin F. Cravatt**[‡,#], **Raymond C. Stevens**[§,#], **Aron H. Lichtman**[x], and **Dale L. Boger**[*,†,#]

[†]Department of Chemistry, The Scripps Research Institute, 10550 North Torrey Pines Road, La Jolla, California 92037

[‡]Department of Chemical Physiology, The Scripps Research Institute, 10550 North Torrey Pines Road, La Jolla, California 92037

[§]Department of Molecular Biology, The Scripps Research Institute, 10550 North Torrey Pines Road, La Jolla, California 92037

[#]The Skaggs Institute for Chemical Biology, The Scripps Research Institute, 10550 North Torrey Pines Road, La Jolla, California 92037

[x]Department of Pharmacology and Toxicology, Virginia Commonwealth University, Richmond, VA 23298

Abstract

The design and characterization of α-ketoheterocycle fatty acid amide hydrolase (FAAH) inhibitors are disclosed that additionally and irreversibly target a cysteine (Cys269) found in the enzyme cytosolic port while maintaining the reversible covalent Ser241 attachment responsible for their rapid and initially reversible enzyme inhibition. Two α-ketooxazoles (**3** and **4**) containing strategically placed electrophiles at the C5 position of the pyridyl substituent of **2** (OL-135) were prepared and examined as inhibitors of FAAH. Consistent with the observed time-dependent non-competitive inhibition, the co-crystal X-ray structure of **3** bound to a humanized variant of rat FAAH revealed that **3** was not only covalently bound to the active site catalytic nucleophile Ser241 as a deprotonated hemiketal, but also to Cys269 through the pyridyl C5-substituent, thus providing an inhibitor with dual covalent attachment in the enzyme active site. In vivo characterization of the prototypical inhibitors in mice demonstrate that they raise endogenous brain levels of FAAH substrates to a greater extent and for a much longer duration (>6 h) than the reversible inhibitor **2**, indicating that the inhibitors accumulate and persist in the brain to completely inhibit FAAH for a prolonged period. Consistent with this behavior and the targeted irreversible enzyme inhibition, **3** reversed cold allodynia in the chronic constriction injury model of neuropathic pain in mice for a sustained period (>6 h) beyond that observed with the reversible inhibitor **2**, providing effects that were unchanged over the 1–6 h time course monitored.

Corresponding Author: boger@scripps.edu.

The authors declare no competing financial interest.

Supporting Information. Full experimental details for the synthesis and characterization of the candidate inhibitors and the dose and time-dependent in vivo effects of **3** on lipid amide levels are provided. This material is available free of charge via the Internet at http://pubs.acs.org.

INTRODUCTION

Inhibitors that react sequentially with two nucleophilic residues in enzyme active sites are rare.[1,2] Representative of the examples, a recent inhibitor discovered by pursuing a high-throughput screening lead for *O*-linked *N*-acetylglucosamine transferase was shown to function by cross-linking two active-site catalytic residues.[3] Building on these rare examples and complementary to their serendipitous discovery, we report herein the design and characterization of α-ketoheterocycle-based fatty acid amide hydrolase (FAAH) inhibitors that additionally and irreversibly target a cysteine (Cys269) found in the enzyme's cytosolic port, while maintaining the reversible covalent Ser241 attachment responsible for their rapid and initially reversible enzyme inhibition. In addition to their discovery by structure-guided design rather than serendipity, an in vivo efficacious but short acting FAAH inhibitor is converted into an enzyme inhibitor with a long acting in vivo duration of action.

FAAH[4,5] inactivates several endogenous signaling lipid amides[6–9] including the endogenous cannabinoid (endocannbinoid) anandamide (**1a**)[10–12] and the sleep-inducing substance oleamide (**1b**, Figure 1).[13–16] FAAH's cellular and subcellular distribution is consistent with its role in regulating a growing class of signaling fatty acid amides[9] at their sites of action.[6] Although FAAH is a member of the amidase signature family of serine hydrolases for which there are a number of prokaryotic enzymes, it is the only well characterized mammalian enzyme bearing the family's unusual Ser–Ser–Lys catalytic triad.[17–19]

Due to the therapeutic potential[20] of FAAH inhibitors for the treatment of pain,[21] inflammatory,[22] and sleep disorders,[15,23] there has been wide-spread interest in the development of selective inhibitors of the enzyme.[24] Since FAAH inhibition only potentiates an activated signaling pathway, increasing the endogenous levels of the released lipid signaling molecules only at their sites of action, it provides a temporal and spatial pharmacological control not available to a classical receptor agonist (e.g., cannabinoid receptor agonists). Following early studies with substrate-inspired inhibitors that served to characterize FAAH as a serine hydrolase,[25–33] a series of potent and selective inhibitors that display excellent in vivo activity have been disclosed, serving to support the use of FAAH as a target for therapeutic intervention.[34] The earliest of such inhibitors were α-ketoheterocycles[35–46] that bind to FAAH by reversible hemiketal formation with an active site serine. Many of these competitive inhibitors were found to be potent and selective for FAAH relative to other mammalian serine hydrolases, and members of this class have been shown to exhibit analgesic activity in vivo.[46,47] Of these, **2** (OL-135) emerged as a potent (K_i = 4.7 nM) and selective (>60–300 fold) FAAH inhibitor that induces analgesia and increases endogenous anandamide levels (Figure 2).[47] It exhibits analgesic or anti-inflammatory activity at doses that approach or exceed those of common pain or anti-inflammatory medications.[47] It lacks significant offsite target activity, does not bind cannabinoid (CB1 or CB2) or vanilloid (TRP) receptors, and the in vivo effects are observed without the respiratory depression and dosing desensitization characteristic of opioid administration or the increased feeding and decreased motor control characteristic of cannabinoid agonists.

Herein, we report the examination of two prototypical inhibitors containing strategically placed electrophiles at the pyridyl C5-position of **2** (Figure 2). The modifications were designed to subsequently react with and trap Cys269 found in the enzyme cytosolic port following hemiketal formation of the electrophilic carbonyl of **3** and **4** with the active site Ser241; thus, providing dual-binding inhibitors. Time-dependent inhibition, Lineweaver–Burk kinetic analysis, and irreversibility studies indicate that the inhibitors ultimately function by a non-competitive mechanism rather than the reversible, competitive inhibition observed for **2** and related α-ketoheterocycle inhibitors. X-ray crystallographic

characterization of **3** in complex with r/hFAAH confirms that the inhibitor is covalently bound in the two distinct positions as designed. In vivo characterization of **3** and **4** demonstrate that such inhibitors raise endogenous FAAH substrates levels both to a greater extent and for an extended duration relative to the reversible inhibitor **2**, and that **3** exhibits a sustained longer acting in vivo analgesic effect relative to **2**.

RESULTS AND DISCUSSION

Chemistry

The core of the inhibitors was accessed by Stille coupling[48] of the stannylated oxazole intermediate **5**[46] with the appropriately functionalized 2-chloropyridines (Scheme 1). Subsequent TBS ether deprotection (Bu_4NF) and oxidation of the liberated alcohols with Dess-Martin periodinane[49] (DMP) provided the corresponding α-ketoheterocycles **4** and **10**. The candidate inhibitor **3** was accessed by further modification of the pyridyl C5-substituent of **10**, entailing methoxymethyl (MOM) ether deprotection and subsequent conversion of the resulting primary alcohol **11** to the corresponding bromide **3**.

Enzyme inhibition

X-ray crystallographic structures of r/hFAAH in complex with **2** and related α-ketoheterocycles and their analyses were previously reported.[50–52] Along with verification of the hemiketal linkage of the active site nucleophilic Ser241 to the electrophilic carbonyl and capturing the active site catalytic residues in an in-action state, Cys269 was observed adjacent to the pyridine ring. The cysteine, located proximal to the active site in the cytosolic port near the pyridine of **2**, is spatially oriented to react with a second electrophile placed on C5 of the pyridyl group of the inhibitor. In principle, this might be achieved by either a second slower and irreversible alkylation as envisioned from the benzylic bromide **3** or by a second, potentially reversible addition as envisioned for the otherwise benign nitrile **4**. In both instances and characteristic of an irreversible enzyme inhibitor, the second covalent attachment would be expected to extend the in vivo duration of action of these inhibitors relative to the reversible inhibitor **2**.

The initial characterization of **3** and **4** and their comparison with **2** was conducted using purified recombinant rat FAAH (rFAAH) expressed in *Escherichia coli*[53] at 20–23°C as previously disclosed.[38] The initial rates of hydrolysis (≤10–20% reaction) were monitored using enzyme concentrations at least three times below an initially measured K_i by following the breakdown of ^{14}C-oleamide and K_i values were established as previously described (Dixon plot).[38] Without pre-incubation with the enzyme, the inhibitors **3** (K_i = 3.1 nM) and **4** (K_i = 1.5 nM) exhibited apparent K_i values similar to that observed with **2** (K_i = 4.7 nM) (Figure 3).

Time-dependent enzyme inhibition

Because we expected the second, subsequent Cys269 alkylation to proceed more slowly than the rapid hemiketal formation of the inhibitors, the time-dependent inhibition of FAAH by **3** and **4** was examined alongside that of **2**. As expected, the potency of **2** did not change with inhibitor-enzyme pre-incubation times of 0–6 h, whereas the apparent K_i values of **3** and **4** increased more than 3- to 15-fold, consistent with slow irreversible inhibition of FAAH (Figure 3).

Lineweaver-Burk kinetic analysis

Inhibitor **2** exhibited simple competitive reversible FAAH inhibition by Lineweaver–Burk kinetic analysis[38] (Figure 4A). In contrast and after 3 h of pre-incubation with FAAH, **3** and

4 exhibited non-competitive FAAH inhibition by Lineweaver–Burk analysis (Figure 4B and C), indicative of irreversible enzyme inhibition and consistent with Cys269 alkylation of the benzylic bromide in the case of **3** and thioimidate formation in the case of **4**.

Irreversible enzyme inhibition

Dialysis dilution (4°C, 18 h, 370-fold) of the FAAH-inhibitor mixture following 3 h of preincubation with **2** restored nearly full enzyme activity consistent with its reversible enzyme inhibition, whereas the analogous dialysis dilution of the mixtures containing **3** and **4** remained unchanged, failing to restore FAAH activity, indicative of irreversible enzyme inhibition (Figure 5). It is especially notable that **4**, presumably forming a Cys269 thioimidate adduct with the nitrile, does not appear to be even slowly reversible under these conditions.

Role of the electrophilic carbonyl

While the kinetic behavior and irreversible nature of the inhibitors **3** and **4** are consistent with the targeted irreversible Cys269 alkylation, these analyses alone do not confirm the observation of the designed alkylation or whether it might indicate the involvement of other active site nucleophiles including those of the Ser–Ser–Lys catalytic triad. In addition, the results would not distinguish between a delivered Cys269 active site alkylation with or without continued Ser241 hemiketal participation that would result in cross-linking two nucleophilic active site residues. The hemiketal participation is reversible and conceivably could participate in delivering the inhibitor to Cys269 proximal to the FAAH active site, but not remain engaged during or subsequent to the eventual covalent alkylation. In order to establish the role of the electrophilic carbonyl, the corresponding alcohols **7** and **12**, as well as the methylene derivative **13**, were also examined (Figure 3). These studies establish that the electrophilic carbonyl of **3** and **4**, and its hemiketal formation with Ser241 is central to their relatively rapid (≤1 h) and potent (apparent K_i = 500–200 pM) irreversible inhibition of FAAH. Although the two alcohols **7** and **12** also exhibited a slow time-dependent increase in FAAH inhibition indicative of an active-site binding and delivery of Cys269 alkylation, they remained at least 100-fold less effective than the corresponding ketones at each time point examined. The corresponding methylene derivative **13** was a further 100-fold less effective, being 10,000-fold less effective than **4**.

X-ray co-crystal structure of 3 bound to FAAH

Although these studies provide convincing, albeit indirect, evidence that the benzylic bromide of **3** and nitrile of **4** are effectively delivered to the FAAH active site and alkylate Cys269, they do not establish whether **3** and **4** simply benefit from the electrophilic hemiketal formation or whether it remains intact in the bound inhibitor. That is, it was still not clear whether the reversible hemiketal formation simply participates in delivering the inhibitor to Cys269, or whether it remains intact during or subsequent to the putative benzylic bromide Cys269 alkylation. In effort to better understand the structural details of **3** binding in the FAAH active site, the complex was crystallographically characterized. The X-ray structure of bromide **3** bound to h/rFAAH[54] was solved to 2.3 Å resolution, with the data processing and refinement statistics reported in Table 1.

Beautifully, inhibitor **3** was found covalently attached to the catalytic Ser241 residue through its electrophilic carbonyl bound as a deprotonated hemiketal mimicking the enzymatic tetrahedral intermediate, a hallmark of the α-ketoheterocycle class of FAAH inhibitors. More importantly, a second covalent attachment between the methylene at C5 of the pyridine and Cys269 is also clearly observed in the electron density (Figure 6). This

presumably occurs through S_N2 displacement of the primary bromide following Ser241 hemiketal formation.

The overlay of the co-crystal structures of **3** and **2**[50] are essentially identical, indicating that capture of the second, irreversible Cys269 alkylation of the benzylic bromide does not distort the inhibitor binding from that observed with **2** (Figure 7). Even the precise positioning of Cys269 is unperturbed in the covalent complex with **3** in comparison to both its position and orientation in complex with **2**, which lacks the covalent thioether bond. Consequently, the reversible Ser241 hemiketal covalent attachment to the electrophilic carbonyl inhibitor remains unperturbed. This results in an exquisite cross-linking at the FAAH active site, wherein covalent, reversible hemiketal formation drives a subsequent slower irreversible Cys269 covalent reaction. That we also observed time-dependent inhibition with **4** further indicates that covalent modification of Cys269 can even occur with electrophiles as benign as a nitrile without disturbing the reversible covalent hemiketal.

Of note, Gly268–Cys269 in the FAAH cytosolic port define an anion binding site that represents a key interaction for specific classes of emerging FAAH substrates (*N*-acyl taurines)[55] and perhaps others yet to be discovered. As illustrated herein, it represents a site unique to FAAH that can be exploited to enhance the potency or selectivity of FAAH inhibitors. In addition to the hemiketal formation observed with **3** and its exquisite interaction with the oxyanion hole defined by Ile238, Gly239, Gly240, and Ser241 and the unusual Ser217-mediated OH-πH-bond to the activating oxazole of **3**, the key anchoring terminal phenyl group of the C2 acyl chain overlays nicely with that of **2** benefiting from the same CH-π interactions.[50–52] The oxazole and pyridyl rings are quasi-coplanar with the pyridyl nitrogen directed toward the oxazole aryl CH rather than oxygen (*anti* vs *syn*). This strongly preferred orientation avoids a destabilizing electrostatic interaction between the pyridyl nitrogen and oxazole oxygen lone pairs while maintaining the stabilizing conjugation between the two aromatic rings.[56] The Thr236 side chain hydroxyl group is oriented toward the pyridyl nitrogen atom of **3** at a distance consistent with a bridging hydrogen-bonded water molecule, although it was not observed in the electron density. Thr236 is H-bonded to Lys142, which is an integral member of the Ser241–Ser217–Lys142 catalytic triad. This intricate H-bonding network, which locks the pyridyl ring into a fixed location and orientation, serves to enhance inhibitor affinity 20-fold.[38] In FAAH complexes with **3** and **4**, it also serves to preposition the pyridyl C5-electrophile for reaction with Cys269.

Inhibitor selectivity

Activity-based protein profiling (ABPP), which uses active site-directed chemical probes to evaluate the activity of enzymes in native biological systems, has emerged as a powerful tool for evaluating candidate serine hydrolase inhibitors directly in complex proteomes.[57] ABPP methods offer the advantage of testing enzymes in their native state and eliminate the need for their recombinant expression, purification, and the development of specific substrate assays. Because inhibitors are screened against many enzymes in the proteome in parallel, both potency and selectivity can be simultaneously evaluated. Previous studies[29] have shown that the α-ketoheterocycle class of inhibitors are exquisitely selective for FAAH, although two enzymes did emerge as potential competitive targets: triacylglycerol hydrolase (TGH) and the membrane-associated hydrolase, KIAA1363. Each inhibitor (**3** and **4**) was tested for its effects on the fluorophosphonate (FP)-rhodamine probe labeling of serine hydrolases in the mouse brain (Figure 8) and heart membrane proteome (Supporting Information) at concentrations ranging from 10 nM to 100 μM. As observed in previous studies, inhibitors **3** and **4** showed excellent selectivity for FAAH over KIAA1363 (>10^3 fold) and good selectivity over TGH (Supporting Information Figure S2) with a 20 min

inhibitor preincubation, where FAAH inhibition may still be reversible. As expected, the activity against KIAA1363 did not change with the 6 h incubation consistent with a reversible interaction with the inhibitors. Similarly, competitive inhibition of monoacylglycerol lipase (MAGL) and α,β-hydrolase containing domain 6 (ABHD6) was observed only at concentrations 10^2–10^3 times higher than that required to inhibit labeling of FAAH. This selectivity (>10^4–10^5 fold vs KIAA1363,>10 fold vs TGH,>10^2 fold vs MAGL,>10^4 fold vs ABHD6), as well as FAAH potency (>10-fold), increased with the more prolonged 6 h preincubation with inhibitor where FAAH inhibition is irreversible (Figure 8). Only MAGL, which acts on a similar substrate and is known to possess at least one reactive active site cysteine,[58] appears to exhibit a weaker (>100-fold) but time-dependent increase in potency at 6 h with inhibitor **4**. Other significant off target inhibition was only observed at 20 min or 6 h at inhibitor concentrations of 100 μM, a concentration that is >10^4-fold over the concentration at which **3** and **4** inhibit FAAH.

A subtle impact of the nature of the pyridyl C5 substituent is also apparent in this proteome-wide assay with **4** displaying a greater potency than **3** at both time points. This may be reflective of some non-productive consumption of the more reactive benzylic bromide **3** compared to the otherwise benign nitrile **4** in the proteome millue. Nonetheless and even under such conditions, both the inhibitor **3** containing a reactive benzylic bromide as well as the inhibitor **4** containing a relatively unreactive nitrile exhibit good FAAH selectivity even after 6 h preincubation with mouse brain membrane proteome. In this assay, both inhibitors exhibit a slow time-dependent increase in potency (6 h > 20 min) reflective of their slow irreversible enzyme inhibition, displaying IC_{50} values <10 nM (**4** > **3**) after the 6 h pre-incubation. Notably, the addition of a second and slow covalently modifying functionality did not erode, and may have additionally enhanced, the inhibitor selectivity, especially upon prolonged proteome exposure.

Preliminary in vivo characterization

In initial efforts to establish in vivo inhibition of FAAH and its subsequent pharmacological effects, the inhibitors **3** and **4** were examined alongside **2** for their ability to increase the endogenous levels of a series of lipid amide signaling molecules in both the brain (CNS effect) and liver (peripheral effect). This entailed monitoring the effects of the inhibitors on the endogenous levels of the FAAH substrates anandamide (AEA), oleoyl ethanolamide (OEA), and palmitoyl ethanolamide (PEA). It is the increase in endogenous levels of anandamide (AEA) in the brain and its subsequent action at cannabinoid (CB1 and CB2) receptors that are thought to be responsible for the analgesic effects of FAAH inhibitors. The effects were established at two time points (1 and 3 h) following intraperitoneal (i.p.) administration of 30 mg/kg inhibitor in a single mouse per time point for the initial screen. Both inhibitors **3** and **4** increased the endogenous levels of the key lipid amides in both the brain and liver (not shown). In addition, these effects appeared to not only persist over the 3 h time course, but they were also greater in magnitude relative to **2**.

As a result, a dose- and time-dependent study of the effect of **4** on the endogenous brain levels of AEA, OEA, and PEA was conducted. Compound **4** was administered to mice (10, 30 and 50 mg/kg, i.p., two mice at each dose) and the animals were sacrificed at various time points up to 6 h post-administration. Brains from these mice were analyzed for FAAH substrate levels. Compound **4** increased the levels of AEA (2–4 fold at 30 and 50 mg/kg) in a dose-dependent manner with maximum increases still observed 6 h after administration (Figure 9A). Significant in these observations is the fact that partial blockage of FAAH in vivo can cause elevations in PEA and OEA, but >90% FAAH inhibition is required to elevate AEA levels in vivo.[59c] Brain levels of palmitoyl ethanolamide and oleoyl ethanolamide also increased in a dose-dependent manner. After 1 h, levels of PEA increased

5.9-fold and levels of OEA increased 4.5-fold (Figure 9B and C). Moreover these levels continued to rise 3 h post administration of **4** (PEA increases 12-fold). These elevations exceeded the effects observed with **2** in earlier studies with administration at 50 mg/kg[46] where both the maximum lipid amide increase is lower and the duration of the increase is much shorter (1 h max). Consequently, a side-by-side comparison of **4** with **2** was also conducted, measuring the impact **2** had on the same signaling amides when also administered at 30 mg/kg (i.p.). Since the effects of **2** had been previously established to dissipate by 6 h, measurements of the effects of **2** where recorded at 1 and 3 h. As shown in Figure 10, the maximum effect of **2** on all three lipid amides is observed at 1 h, is already attenuated at 3 h, and can be projected from the trends to have dissipated at 6 h as previously observed.[46] Since **2** has been shown to exhibit good brain exposure effectively crossing the blood brain barrier such that plasma and brain concentrations are equivalent,[46] the distinctions in the in vivo activity of **2** versus **4** (or **3**) are not due to poor brain exposure to **2** (Supporting Information Figure S3). Both the duration (>6 h for **4**) and the magnitude of the lipid amide elevations is much more robust with **4** versus **2**. Thus, administration of **4** caused substantial accumulations of all three measured FAAH substrates in brain, with peak levels of AEA achieved within 1.5–3 h (Figure 11A and B), and elevations in these lipids were maintained over the 6 h time course, similar to the behavior of irreversible carbamate inhibitors of FAAH such as URB597 and PF-3845.[59–61] The impact of the benzylic bromide **3** at 30 mg/kg (i.p.) in increasing brain levels of AEA was also examined and found to be indistinguishable from that of the nitrile **4** (data in Supporting Information Figure S1). These sustained and long lasting increases in the in vivo lipid amide levels indicate that inhibitors **4** and **3** achieve sufficiently high brain levels after its initial dosing to produce durable (>6 h) and near-complete inhibition of FAAH (>90%), consistent with their slow irreversible inhibition of FAAH.

Inhibitor 3 exhibits a sustained in vivo duration of action in a model of neuropathic pain

In an important extension of the studies and following observation of the long-acting in vivo effects on endogenous AEA levels following i.p. administration, mice were subjected to chronic constriction injury (CCI) and examined 14 days later for signs of neuropathic pain. Inhibitor **3**, administered i.p. (30 mg/kg), significantly attenuated cold allodynia in paws ipsilateral to CCI surgery, exhibiting a maximal efficacy that matches that observed with the reversible inhibitor **2** (OL-135) but with a much longer duration of action (Figure 12). In the control paws of the same mice, **3** had no effect on cold allodynia indicating a lack of effects (e.g., sedative) on the uninjured paws. Significantly, the effects of **3** following its administration were sustained, remaining unchanged over the 1–6 h time course monitored and indicating a pronounced in vivo efficacy lasting >6 h. This contrasts the shorter duration of action of the reversible inhibitor **2** whose in vivo effects dissipated over this time course.

CONCLUSIONS

The design of α-ketohetorocycles additionally targeting the remote Cys269 found in the cytosolic port of FAAH provided inhibitors that covalently react with two active site nucleophiles. The cross-link design was sufficiently accurate that the first of the two covalent attachments, the hemiketal, while being itself reversible, remains intact after the second, slower irreversible reaction with Cys269. The second electrophile targeting Cys269 was incorporated as a C5 substituent on the pyridyl group of 5-(pyrid-2-yl)oxazoles including **2**, and ranged from the irreversibly reactive benzylic bromide **3** to the covalent reversible and typically benign nitrile **4**. Consistent with expectations, the inhibitors exhibited time-dependent, non-competitive enzyme inhibition, produced sustained accumulation of the endogenous substrates for FAAH in vivo for >6 h, and exhibited efficacious and long-acting antinociceptive activity (>6 h) in an in vivo model of

neuropathic pain. The exquisite FAAH active site cross-linking by **3** was confirmed by X-ray crystallography, unambiguously establishing it as a rare example of sequential reaction of an inhibitor with two nucleophiles in the active site of an enzyme,[1–3] and the only characterized example, to our knowledge, where both the cross-linking was achieved through rational, structure-guided design and where one of the covalent attachments is reversible. Our studies thus serve as a prototype for an approach to convert selective short-acting reversible, competitive serine hydrolase inhibitors into in vivo efficacious compounds that produce a robust long-acting pharmacological response suitable for target validation or drug development by targeting peripheral active site nucleophiles.

EXPERIMENTAL

FAAH Inhibition

^{14}C-labeled oleamide was prepared from ^{14}C-labeled oleic acid as described.[15] The truncated rat FAAH (rFAAH) was expressed in *E. coli* and purified as described.[53] The purified recombinant rFAAH was used in the inhibition assays. The inhibition assays were performed as described.[15] The enzyme reaction was initiated by mixing 1 nM of rFAAH (800, 500, or 200 pM rFAAH for inhibitors with $K_i \leq 1–2$ nM) with 20 μM of ^{14}C-labeled oleamide in 500 μL of reaction buffer (125 mM TrisCl, 1 mM EDTA, 0.2% glycerol, 0.02% Triton X-100, 0.4 mM Hepes, pH 9.0) at room temperature in the presence of three different concentrations of inhibitor. The enzyme reaction was terminated by transferring 20 μL of the reaction mixture to 500 μL of 0.1 N HCl at three different time points. The ^{14}C-labeled oleamide (substrate) and oleic acid (product) were extracted with EtOAc and analyzed by TLC as detailed. The K_i of the inhibitor was calculated using a Dixon plot as described (standard deviations are provided in the Supporting Information tables). Lineweaver–Burk analysis was performed as described confirming competitive, reversible inhibition for **2**, and non-competitive inhibitions for **3** and **4** (Figures 4A, B, and C).

Reversibility of FAAH Inhibition (Dialysis)

The reversibility of FAAH inhibition by **2**, **3** and **4** was assessed by dialysis dilution using recombinant rFAAH. Cell pellets were homogenized in 15 mL FAAH assay buffer (125 mM Tris, 1 mM EDTA, 0.2% glycerol, 0.02% Triton X-100, 0.4 mM Hepes, pH 9.0). A 3 mL aliquot of membrane homogenate was used for each sample dialyzed. The dialysis experiment was performed in the pre-dialysis mix at or near the apparent IC_{80}. The final assay inhibitor concentrations used were 100 nM **2**, 80 nM **3**, and 80 nM **4**. Samples were pre-incubated with the enzyme for 3 h at room temperature (22°C) before 300 μL was removed and assayed in triplicate in a FAAH activity assay. The remaining sample (2.7 mL) was injected into a dialysis cassette employing a 10,000 MW cutoff membrane. The mixture was dialyzed against 1 L PBS at 4 °C on a stir plate for 18 h. The post dialysis FAAH activity was assessed by assaying 300 μL samples taken from the dialysis cassettes in triplicate. FAAH activity is expressed as a percentage of vehicle treated FAAH (DMSO alone).

Competitive ABPP of FAAH inhibitors with FP-rhodamine

Mouse tissues were Dounce-homogenized in PBS buffer (pH 8.0) and membrane proteomes isolated by centrifugation at 4 °C (100,000*g*, 45 min), washed, resuspended in PBS buffer, and adjusted to a protein concentration of 1 mg/mL. Proteomes were preincubated with inhibitors (10–100,000 nM; DMSO stocks) for 20 min and 6 h and then treated with FP-rhodamine (100 nM, DMSO stock) at room temperature for 10 min. Reactions were quenched with SDS-PAGE loading buffer, subjected to SDS-PAGE, and visualized in-gel using flatbed fluorescence scanner (MiraBio). Labeled proteins were quantified by measuring integrated band intensities (normalized for volume); control samples (DMSO

alone) were considered 100% activity. IC_{50} values were determined from dose-response curves using Prism software.

In vivo Pharmacodynamic Studies with Inhibitors

Inhibitors were prepared as a saline-emulphor emulsion for intraperitoneal (i.p.) administration by vortexing, sonicating, and gently heating neat compound directly into an 18:1:1 v/v/v solution of saline:ethanol:emulphor. Male C57Bl/6J mice (<6 months old, 20–28 g) were administered inhibitors in saline-emulphor emulsion or an 18:1:1 v/v/v saline:emulphor:ethanol vehicle i.p. at a volume of 10 μL/g weight. After the indicated amount of time (1, 3, and 6 h), mice were anesthetized with isofluorane and decapitated. Total brains (~400 mg) and a portion of the liver (~100 mg) were removed and flash frozen in liquid N_2. Animal experiments were conducted in accordance with the guidelines of the Institutional Animal Care and Use Committee of The Scripps Research Institute.

Measurement of Brain Lipids

Tissue was weighed and subsequently Dounce homogenized in 2:1:1 v/v/v $CHCl_3$:MeOH:Tris pH 8.0 (8 mL) containing standards for lipids (50 pmol d_4-PEA, 2 pmol d_4-AEA, and 10 nmol pentadecanoic acid). The mixture was vortexed and then centrifuged (1,400 × *g*, 10 min). The organic layer was removed, evaporated under a stream of N_2, resolubilized in 2:1 v/v $CHCl_3$:MeOH (120 μL), and 10 μL of this resolubilized lipid solution was injected onto an Agilent G6410B QQQ instrument. LC separation was achieved with a Gemini reverse-phase C18 column (5 μm, 4.6 mm × 50 mm, Phenomonex) together with a pre-column (C18, 3.5 μm, 2 mm × 20 mm). Mobile phase A was composed of a 95:5 v/v H_2O:MeOH, and mobile phase B was composed of a 65:35:5 v/v/v *i*-PrOH:MeOH:H_2O. 0.1% Formic acid or 0.1% ammonium hydroxide was included to assist in ion formation in positive and negative ionization mode, respectively. The flow rate for each run started at 0.1 mL/min with 0% B. At 5 min, the solvent was immediately changed to 60% B with a flow rate of 0.4 mL/min and increased linearly to 100% B over 10 min. This was followed by an isocratic gradient of 100% B for 5 min at 0.5 mL/min before equilibrating for 3 min at 0% B at 0.5 mL/min (23 min total per sample). MS analysis was performed with an electrospray ionization (ESI) source. The following MS parameters were used to measure the indicated metabolites in positive mode (precursor ion, product ion, collision energy in V): AEA (348, 62, 11), OEA (326, 62, 11), PEA (300, 62, 11), d_4-AEA (352, 66, 11), d_4-PEA (304, 62, 11). For negative polarity, the analysis was performed in MS2 scan mode from 100–1000 *m*/*z*. The capillary was set to 4 kV, the ionization source was set to 100 V, and the delta EMV was set to 0. Lipids were quantified by measuring the area under the peak in comparison to the standards.

Chronic Constriction Injury (CCI) Allodynia Assay

Surgery was performed as described previously.[62] Allodynia was initially tested a minimum of 14 days after surgery. Male C57BL/6 mice were habituated to the test apparatus for 2 h on the 2 days prior to testing. On test days, the mice were brought into the test room, weighed, and allowed to acclimate for at least 1 h before the start of the experiment. Mice were administered inhibitors **2** or **3** (30 mg/kg, n = 10) or vehicle (i.p.) as detailed above, then placed in ventilated polycarbonate cylinders on a mesh table. A within subject design was used in which the mice were administered the different regimens in a counter-balanced fashion, with at least one week between test days. Cold (acetone-induced) allodynia were tested at 1, 3, and 6 h post drug administration. Testing was carried out by an observer who was blinded to treatment conditions. Cold allodynia was tested by propelling 10 μL of acetone (Fisher Bioscience) via air burst, from a 200 μL pipette (Rainin Instruments,

Oakland, CA) onto the plantar surface of each hind paw. Total time lifting or clutching each paw was recorded, with a maximum time of 20 s.[63]

Data Analyses

Behavioral data were analyzed using a two-way mixed factorial analysis of variance (ANOVA) for each paw, with drug treatment as the between subjects measure, and time as the within subjects measure. Follow-up comparisons were made using the Bonferroni test. All animals (n = 10 per treatment group) were included in the analyses. Differences between groups were considered statistically significant at $p < 0.05$.

FAAH Production, Crystallization, and Crystal Structure Determination

The N-terminal transmembrane-deleted humanized version of FAAH (amino acids 32–579) was expressed in *E. coli* and purified as previously described,[54] using 0.08% *n*-undecyl-β-D-maltoside in the ion exchange and size exclusion chromatography steps of the purification. Purified protein was crystallized as previously described,[52] with the modifications described below. Precipitant solution contained 50 mM MES pH 5.5, 0.02% UM-LA, 15% PEG 400, 4% polypropylene glycol P400, 13% xylitol, 1 mM DTT, 50 mM KCl, and 50 mM NaF. Crystals were grown by the sitting drop vapor diffusion method at 14 °C in 96-well plates (Innovaplate SD-2; Innovadyne Technologies), and frozen in liquid nitrogen immediately after harvesting. Crystallographic data was collected at 100 K using the Blu-Ice data collection suite[64] at the Stanford Synchrotron Radiation Laboratory on beam line 11-1, and processed using HKL2000.[65] The structure was determined to 2.30 Å resolution in the space group $P3_221$ by molecular replacement using FAAH coordinates from PDB code 3K84. Molecular replacement and structure refinement were conducted using Phaser[66] and REFMAC[67], respectively, from the CCP4 software suite.[68] The Dundee PRODRG Web server[69] was used to calculate restraint parameters for the covalently bound inhibitor **3**. Crystallographic model building was conducted using Coot,[70] and images of the structure were prepared in PyMOL (DeLano Scientific, LLC). Results from data processing and structure refinement are provided in Table 1. Coordinates for the structure have been deposited in the RCSB Protein Data Bank with accession code 4J5P.

Supplementary Material

Refer to Web version on PubMed Central for supplementary material.

Acknowledgments

We gratefully acknowledge the financial support of the National Institutes of Health (DA015648, DLB; DA017259 and DA033760, BFC; DA017259, RCS; DA009789 and DA017259, AHL).

ABBREVIATIONS

AA	arachidonic acid
ABHD6	αβhydrolase containing domain 6
ABPP	activity-based protein profiling
AEA	anandamide
CB	cannabinoid
CCI	chronic constriction injury
CNS	central nervous system

DMP	Dess-Martin Periodinane
FAAH	fatty acid amide hydrolase
i.p	intraperitoneal
MAGL	monoacylglycerol lipase
OEA	oleoyl ethanolamide
PEA	palmitoyl ethanolamide
TBS	*t*-butyldimethylsilyl
TGH	triacylglycerol hydrolase

References

1. Vijayalakshmi J, Meyer EF Jr, Kam CM, Powers JC. Biochemistry. 1991; 30:2175–2183. [PubMed: 1998677]
2. Drawz SM, Bonomo RA. Clin Microbiol Rev. 2010; 23:160–201. [PubMed: 20065329]
3. Jiang J, Lazarus MB, Pasquina L, Sliz P, Walker S. Nat Chem Biol. 2012; 8:72–77. [PubMed: 22082911]
4. Cravatt BF, Giang DK, Mayfield SP, Boger DL, Lerner RA, Gilula NB. Nature. 1996; 384:83–87. [PubMed: 8900284]
5. Giang DK, Cravatt BF. Proc Natl Acad Sci USA. 1997; 94:2238–2242. [PubMed: 9122178]
6. Patricelli MP, Cravatt BF. Vit Hormones. 2001; 62:95–131.
7. Egertova M, Cravatt BF, Elphick MR. Neuroscience. 2003; 119:481–496. [PubMed: 12770562]
8. Boger DL, Fecik RA, Patterson JE, Miyauchi H, Patricelli MP, Cravatt BF. Bioorg Med Chem Lett. 2000; 10:2613–2616. [PubMed: 11128635]
9. Ezzili C, Otrubova K, Boger DL. Bioorg Med Chem Lett. 2010; 20:5959–5968. [PubMed: 20817522]
10. Devane WA, Hanus L, Breuer A, Pertwee RG, Stevenson LA, Griffin G, Gibson D, Mandelbaum A, Etinger A, Mechoulam R. Science. 1992; 258:1946–1949. [PubMed: 1470919]
11. Martin BR, Mechoulam R, Razdan RK. Life Sci. 1999; 65:573–595. [PubMed: 10462059]
12. Schmid HHO, Schmid PC, Natarajan V. Prog Lipid Res. 1990; 29:1–43. [PubMed: 2087478]
13. Boger DL, Henriksen SJ, Cravatt BF. Curr Pharm Des. 1998; 4:303–314. [PubMed: 10197045]
14. Cravatt BF, Lerner RA, Boger DL. J Am Chem Soc. 1996; 118:580–590.
15. Cravatt BF, Prospero–Garcia O, Suizdak G, Gilula NB, Henriksen SJ, Boger DL, Lerner RA. Science. 1995; 268:1506–1509. [PubMed: 7770779]
16. Lerner RA, Siuzdak G, Prospero–Garcia O, Henriksen SJ, Boger DL, Cravatt BF. Proc Natl Acad Sci USA. 1994; 91:9505–9508. [PubMed: 7937797]
17. (a) Patricelli MP, Cravatt BF. Biochemistry. 1999; 38:14125–14130. [PubMed: 10571985] (b) Patricelli MP, Cravatt BF. J Biol Chem. 2000; 275:19177–19184. [PubMed: 10764768] (c) Patricelli MP, Lovato MA, Cravatt BF. Biochemistry. 1999; 38:9804–9812. [PubMed: 10433686] (d) McKinney MK, Cravatt BF. J Biol Chem. 2003; 278:37393–37399. [PubMed: 12734197]
18. McKinney MK, Cravatt BF. Ann Rev Biochem. 2005; 74:411–432. [PubMed: 15952893]
19. Bracey MH, Hanson MA, Masuda KR, Stevens RC, Cravatt BF. Science. 2002; 298:1793–1796. [PubMed: 12459591]
20. (a) Cravatt BF, Lichtman AH. Curr Opin Chem Biol. 2003; 7:469–475. [PubMed: 12941421] (b) Ahn K, McKinney MK, Cravatt BF. Chem Rev. 2008; 108:1687–1707. [PubMed: 18429637] (c) Ahn K, Johnson DS, Cravatt BF. Exp Opin Drug Discov. 2009; 4:763–784.
21. (a) Cravatt BF, Demarest K, Patricelli MP, Bracey MH, Giang DK, Martin BR, Lichtman AH. Proc Natl Acad Sci USA. 2001; 98:9371–9376. [PubMed: 11470906] (b) Lichtman AH, Shelton CC, Advani T, Cravatt BF. Pain. 2004; 109:319–327. [PubMed: 15157693] (c) Cravatt BF,

Saghatelian A, Hawkins EG, Clement AB, Bracey MH, Lichtman AH. Proc Natl Acad Sci USA. 2004; 101:10821–10826. [PubMed: 15247426]

22. Karsak M, Gaffal E, Date R, Wang–Eckhardt L, Rehnelt J, Petrosino S, Starowicz K, Steuder R, Schlicker E, Cravatt BF, Mechoulam R, Buettner R, Werner S, Di Marzo V, Tueting T, Zimmer A. Science. 2007; 316:1494–1497. [PubMed: 17556587]
23. (a) Huitrón–Reséndiz S, Gombart L, Cravatt BF, Henriksen SJ. Exp Neurol. 2001; 172:235–243. [PubMed: 11681856] (b) Huitrón–Reséndiz S, Sanchez–Alavez M, Wills DN, Cravatt BF, Henriksen SJ. Sleep. 2004; 27:857–865. [PubMed: 15453543]
24. Clement AB, Hawkins EG, Lichtman AH, Cravatt BF. J Neurosci. 2003; 23:3916–3923. [PubMed: 12736361]
25. Patricelli MP, Patterson JP, Boger DL, Cravatt BF. Bioorg Med Chem Lett. 1998; 8:613–618. [PubMed: 9871570]
26. Koutek B, Prestwich GD, Howlett AC, Chin SA, Salehani D, Akhavan N, Deutsch DG. J Biol Chem. 1994; 269:22937–22940. [PubMed: 8083191]
27. Patterson JE, Ollmann IR, Cravatt BF, Boger DL, Wong CH, Lerner RA. J Am Chem Soc. 1996; 118:5938–5945.
28. Boger DL, Sato H, Lerner AE, Austin BJ, Patterson JE, Patricelli MP, Cravatt BF. Bioorg Med Chem Lett. 1999; 9:265–270. [PubMed: 10021942]
29. Leung D, Hardouin C, Boger DL, Cravatt BF. Nat Biotech. 2003; 21:687–691.
30. Deutsch DG, Omeir R, Arreaza G, Salehani D, Prestwich GD, Huang Z, Howlett A. Biochem Pharmacol. 1997; 53:255–260. [PubMed: 9065728]
31. Deutsch DG, Lin S, Hill WAG, Morse KL, Salehani D, Arreaza G, Omeir RL, Makriyannis A. Biochem Biophys Res Commun. 1997; 231:217–221. [PubMed: 9070252]
32. Edgemond WS, Greenberg MJ, McGinley PJ, Muthians S, Campbell WB, Hillard CJ. J Pharmacol Exp Ther. 1998; 286:184–190. [PubMed: 9655859]
33. Du W, Hardouin C, Cheng H, Hwang I, Boger DL. Bioorg Med Chem Lett. 2005; 15:103–106. [PubMed: 15582420]
34. (a) Otrubova K, Ezzili C, Boger DL. Bioorg Med Chem Lett. 2011; 21:4674–4685. [PubMed: 21764305] (b) Deng HF. Exp Opin Drug Discov. 2010; 5:961–993.(c) Seierstad M, Breitenbucher JG. J Med Chem. 2008; 51:7327–7343. [PubMed: 18983142] (d) Vandevoorde S. Curr Top Med Chem. 2008; 8:247–267. [PubMed: 18289091]
35. Otrubova K, Boger DL. ACS Chem Neurosci. 2012; 3:340–348. [PubMed: 22639704]
36. Boger DL, Sato H, Lerner AE, Hedrick MP, Fecik RA, Miyauchi H, Wilkie GD, Austin BJ, Patricelli MP, Cravatt BF. Proc Natl Acad Sci USA. 2000; 97:5044–5049. [PubMed: 10805767]
37. Boger DL, Miyauchi H, Hedrick MP. Bioorg Med Chem Lett. 2001; 11:1517–1520. [PubMed: 11412972]
38. Boger DL, Miyauchi H, Du W, Hardouin C, Fecik RA, Cheng H, Hwang I, Hedrick MP, Leung D, Acevedo O, Guimarães CRW, Jorgensen WL, Cravatt BF. J Med Chem. 2005; 48:1849–1856. [PubMed: 15771430]
39. Leung D, Du W, Hardouin C, Cheng H, Hwang I, Cravatt BF, Boger DL. Bioorg Med Chem Lett. 2005; 15:1423–1428. [PubMed: 15713400]
40. Romero FA, Hwang I, Boger DL. J Am Chem Soc. 2006; 68:14004–14005. [PubMed: 17061864]
41. Romero FA, Du W, Hwang I, Rayl TJ, Kimball FS, Leung D, Hoover HS, Apodaca RL, Breitenbucher BJ, Cravatt BF, Boger DL. J Med Chem. 2007; 50:1058–1068. [PubMed: 17279740]
42. Hardouin C, Kelso MJ, Romero FA, Rayl TJ, Leung D, Hwang I, Cravatt BF, Boger DL. J Med Chem. 2007; 50:3359–3368. [PubMed: 17559203]
43. Kimball FS, Romero FA, Ezzili C, Garfunkle J, Rayl TJ, Hochstatter DG, Hwang I, Boger DL. J Med Chem. 2008; 51:937–947. [PubMed: 18247553]
44. Garfunkle J, Ezzili C, Rayl TJ, Hochstatter DG, Hwang I, Boger DL. J Med Chem. 2008; 51:4393–4403.
45. DeMartino JK, Garfunkle J, Hochstatter DG, Cravatt BF, Boger DL. Bioorg Med Chem Lett. 2008; 18:5842–5846. [PubMed: 18639454]

46. Ezzili C, Mileni M, McGlinchey N, Long JZ, Kinsey SG, Hochstatter DG, Stevens RC, Lichtman AH, Cravatt BF, Bilsky EJ, Boger DL. J Med Chem. 2011; 113:7277–7287.
47. (a) Lichtman AH, Leung D, Shelton CC, Saghatelian A, Hardouin C, Boger DL, Cravatt BF. J Pharmacol Exp Ther. 2004; 311:441–448. [PubMed: 15229230] (b) Chang L, Luo L, Palmer JA, Sutton S, Wilson SJ, Barbier AJ, Breitenbucher JG, Chaplan SR, Webb M. Br J Pharmacol. 2006; 148:102–113. [PubMed: 16501580] (c) Schlosburg JE, Boger DL, Cravatt BF, Lichtman AH. J Pharmacol Exp Ther. 2009; 329:314–323. [PubMed: 19168707] (d) Kinsey SG, Long JZ, O'Neal ST, Abdulla RA, Poklis JL, Boger DL, Cravatt BF, Lichtman AH. J Pharmacol Exp Ther. 2009; 330:902–910. [PubMed: 19502530] (e) Booker L, Kinsey SG, Abdullah RA, Blankman JL, Long JZ, Boger DL, Cravatt BF, Lichtman AH. Br J Pharmacol. 2012; 165:2485–2496. [PubMed: 21506952]
48. Farina V, Krishnamurthy V, Scott WJ. Org React. 1997; 50:1–652.
49. Dess DB, Martin JC. J Am Chem Soc. 1991; 113:7277–7287.
50. Mileni M, Garfunkle J, DeMartino JK, Cravatt BF, Boger DL, Stevens RC. J Am Chem Soc. 2009; 131:10497–10506. [PubMed: 19722626]
51. Mileni M, Garfunkle J, Kimball FS, Cravatt BF, Stevens RC, Boger DL. J Med Chem. 2010; 53:230–240. [PubMed: 19924997]
52. Mileni M, Garfunkle J, Ezzili C, Cravatt BF, Stevens RC, Boger DL. J Am Chem Soc. 2011; 133:4092–4100. [PubMed: 21355555]
53. Patricelli MP, Lashuel HA, Giang DK, Kelly JW, Cravatt BF. Biochemistry. 1998; 37:15177–15187. [PubMed: 9790682]
54. Mileni M, Johnson DS, Wang Z, Everdeen DS, Liimatta M, Pabst B, Bhattacharya K, Nugent RA, Kamtekar S, Cravatt BF, Ahn K, Stevens RC. Proc Natl Acad Sci USA. 2008; 105:12820–12824. [PubMed: 18753625]
55. (a) McKinney MK, Cravatt BF. Biochemistry. 2006; 45:9016–9022. [PubMed: 16866346] (b) Saghatelian A, McKinney MK, Bandell M, Patapoutian A, Cravatt BF. Biochemistry. 2006; 45:9007–9015. [PubMed: 16866345] (c) Saghatelian A, Trauger SA, Want EJ, Hawkins EG, Suizdak G, Cravatt BF. Biochemistry. 2004; 43:14332–14339. [PubMed: 15533037]
56. Guimaráes CRW, Boger DL, Jorgensen WL. J Am Chem Soc. 2005; 127:17377–17384. [PubMed: 16332087]
57. Evans MJ, Cravatt BF. Chem Rev. 2006; 106:3279–3301. [PubMed: 16895328]
58. (a) Saario SM, Salo OMH, Nevalainen T, Poso A, Laitinen JT, Järvinen T, Niemi R. Chem Biol. 2005; 12:649–656. [PubMed: 15975510] (b) Labar G, Bauvois C, Borel F, Ferrer JL, Wouters J, Lambert DM. Chem Bio Chem. 2010; 11:218–227.(c) Zvonok N, Pandarinathan L, Williams J, Johnston M, Karageorgos I, Janero DR, Krishnan SC, Makriyannis A. Chem Biol. 2008; 15:854–862. [PubMed: 18721756] (d) King AR, Lodola A, Carmi C, Fu J, Mor M, Piomelli D. Br J Pharmacol. 2009; 157:974–983. [PubMed: 19486005]
59. (a) Ahn K, Johnson DS, Fitzgerald LR, Liimatta M, Arendse A, Stevenson T, Lund ET, Nugent RA, Normanbhoy T, Alexander JP, Cravatt BF. Biochemistry. 2007; 46:13019–13030. [PubMed: 17949010] (b) Johnson DS, Ahn K, Kesten S, Lazerwith SE, Song Y, Morris M, Fay L, Gregory T, Stiff C, Dunbar JB Jr, Liimatta M, Beidler D, Smith S, Nomanbhoy TK, Cravatt BF. Bioorg Med Chem Lett. 2009; 19:2865–2869. [PubMed: 19386497] (c) Ahn K, Johnson DS, Mileni M, Beidler D, Long JZ, McKinney MK, Weerapana E, Sadagopan N, Liimatta M, Smith SE, Lazerwith S, Stiff C, Kamtekar S, Bhattacharya K, Zhang Y, Swaney S, Van Becelaere K, Stevens RC, Cravatt BF. Chem Biol. 2009; 16:411–420. [PubMed: 19389627] (d) Johnson DS, Stiff C, Lazerwith SE, Kesten SR, Fay LK, Morris M, Beidler D, Liimatta MB, Smith SE, Dudley DT, Sadagopan N, Bhattachar SN, Kesten SJ, Nomanbhoy TK, Cravatt BF, Ahn K. ACS Med Chem Lett. 2011; 2:91–96. [PubMed: 21666860]
60. Alexander JP, Cravatt BF. Chem Biol. 2005; 12:1179–1187. [PubMed: 16298297]
61. (a) Jayamanne A, Greenwood R, Mitchell VA, Aslan S, Piomelli D, Vaughan CW. Br J Pharmacol. 2006; 147:281–288. [PubMed: 16331291] (b) Keith JM, Apodaca R, Xiao W, Seierstand M, Pattabiraman K, Wu J, Webb M, Karbarz MJ, Brown S, Wilson S, Scott B, Tham C–S, Luo L, Palmer J, Wennerholm M, Chaplan S, Breitenbucher JG. Bioorg Med Chem Lett. 2008; 18:4838–4843. [PubMed: 18693015] (c) Karbarz MJ, Luo L, Chang L, Tham C-S, Balmer JA, Wilson SJ, Wennerholm ML, Brown SM, Scott BP, Apodaca RL, Keith JM, Wu J, Breitenbucher JG,

Chaplan SR, Webb M. Anesth Analg. 2009; 108:316–329. [PubMed: 19095868] (d) Keith JM, Apodaca R, Tichenor M, Xiao W, Jones W, Pierce J, Seierstad M, Palmer J, Webb M, Karbarz M, Scott B, Wilson S, Luo L, Wennerholm M, Chang L, Brown S, Rizzolio M, Rynberg R, Chaplan S, Breitenbucher JG. ACS Med Chem Lett. 2012; 3:823–827.

62. Kinsey SG, Long JZ, Cravatt BF, Lichtman AH. J Pain. 2010; 11:1420–1428. [PubMed: 20554481]
63. Decosterd I, Woolf CJ. Pain. 2000; 87:149–158. [PubMed: 10924808]
64. McPhillips TM, McPhillips SE, Chiu HJ, Cohen AE, Deacon AM, Ellis PJ, Garman E, Gonzalez A, Sauter NK, Phizackerley RP, Soltis SM, Kuhn P. J Synchrotron Radiat. 2002; 9:401–406. [PubMed: 12409628]
65. Otwinowski Z, Minor W. Methods Enzymol. 1997; 276:307–326.
66. McCoy AJ, Grosse-Kunstleve RW, Adams PD, Winn MD, Storoni LC, Read RJ. J Appl Cryst. 2007; 40:658–674. [PubMed: 19461840]
67. Murshudov GN, Vagin AA, Dodson EJ. Acta Crystallogr. 1997; D53:240–255.
68. Collaborative Computational Project, Number 4. Acta Crystallogr. 1994; D50:760–763.
69. Schüttelkopf AW, van Aalten DMF. Acta Crystallogr. 2004; D60:1355–1363.
70. Emsley P, Cowtan K. Acta Crystallogr. 2004; D60:2126–2132.

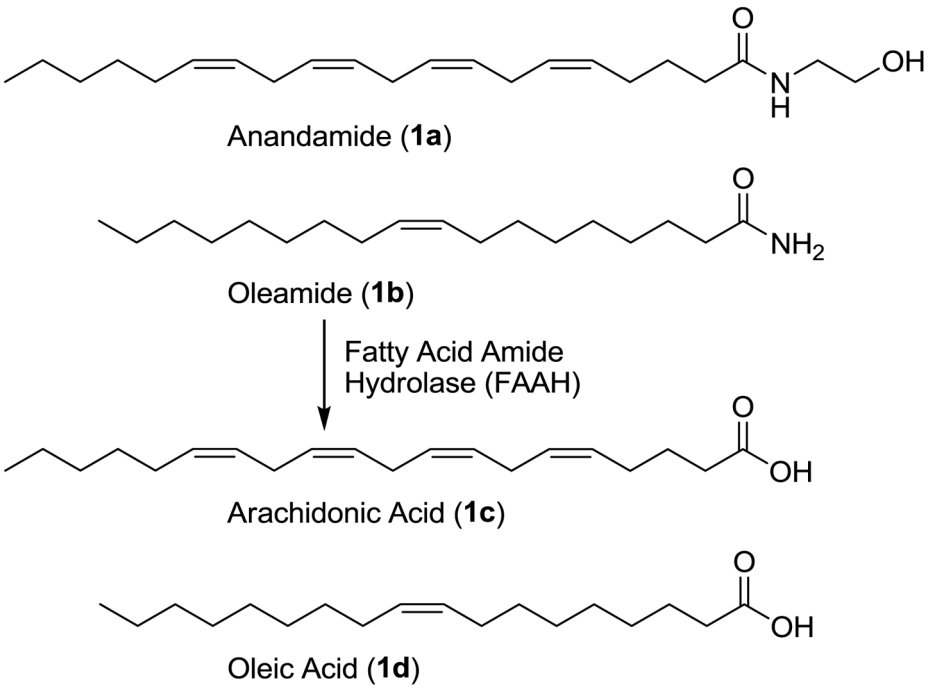

Figure 1.
Endogenous FAAH substrates and corresponding hydrolysis products.

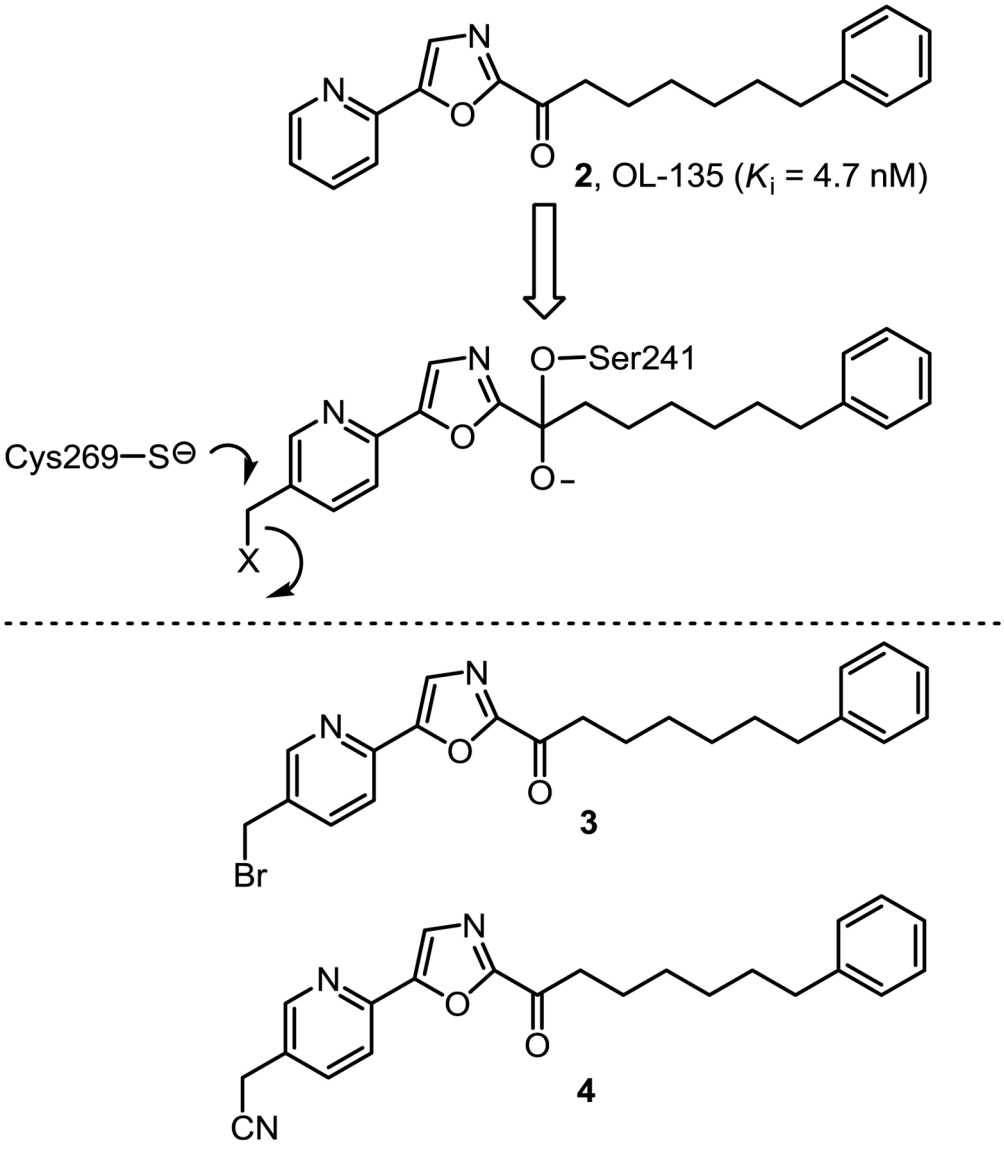

Figure 2.

Design of the active-site cross-linking inhibitors **3** and **4**. Thiophilic electrophiles were placed at the pyridine C5 position of the α-ketoheterocycle inhibitor **2**, proximal to residue Cys269 found in the FAAH cytosolic port.

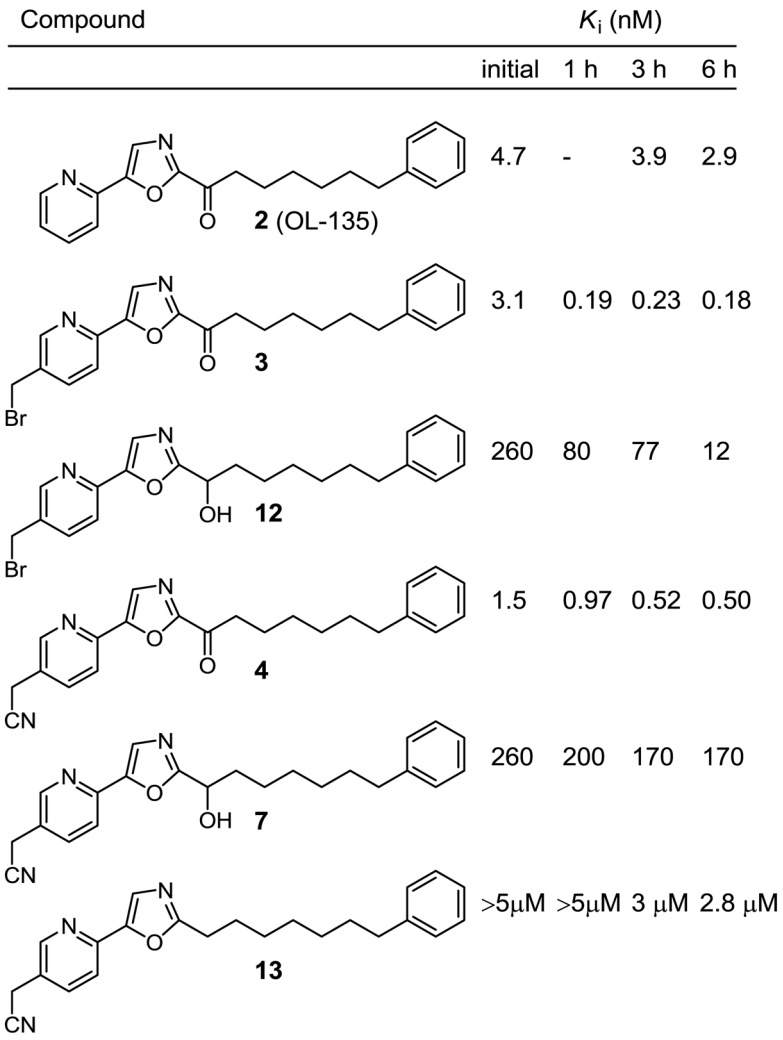

Figure 3.
Time-dependent FAAH inhibition. Apparent K_i values were measured after 0–6 h pre-incubation of inhibitor with rFAAH.

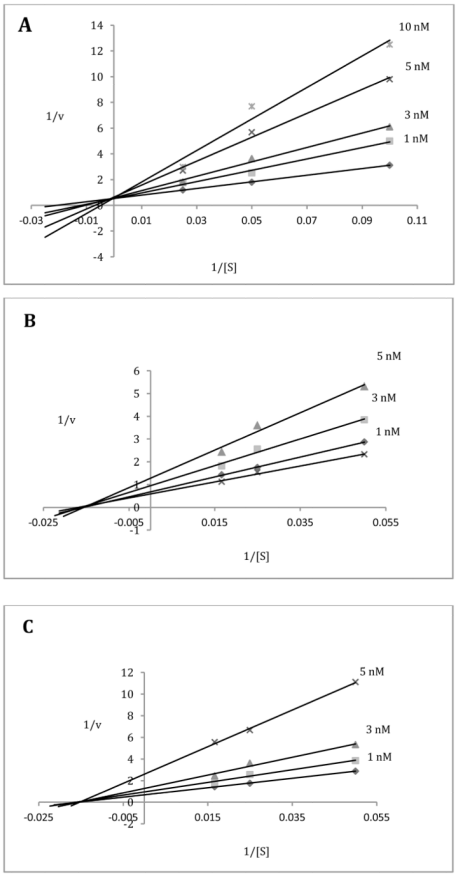

Figure 4.
Lineweaver–Burk analysis demonstrates reversible, competitive inhibition by **2** (A) and the non-competitive inhibition by **3** (B) and **4** (C) after inhibitor-enzyme preincubation for 3 h.

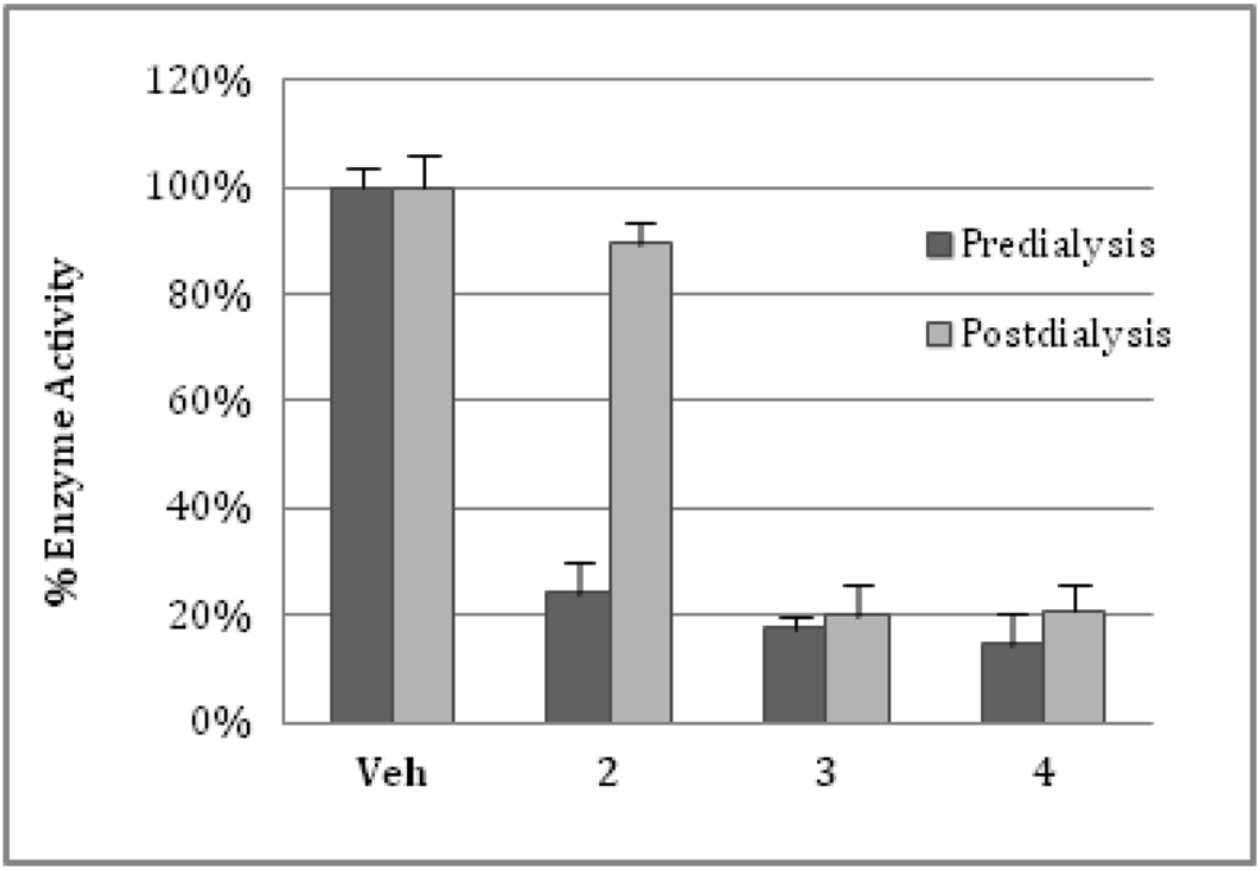

Figure 5.

Dialysis dilution of inhibitor-FAAH mixtures confirms reversible inhibition by **2** and establishes irreversible FAAH inhibition by **3** and **4**. After 3 h preincubation of FAAH with compounds at concentrations that result in inhibition of ca. 80% enzyme activity (22°C, 3 h; 100 nM **2**, 80 nM **3** and **4**) and following measurement of residual enzyme activity, dialysis dilution (4°C, 18 h, 370-fold dilution) of the mixtures resulted in nearly full recovery of enzyme activity for **2**, but little or no recovery of enzyme activity for **3** and **4**.

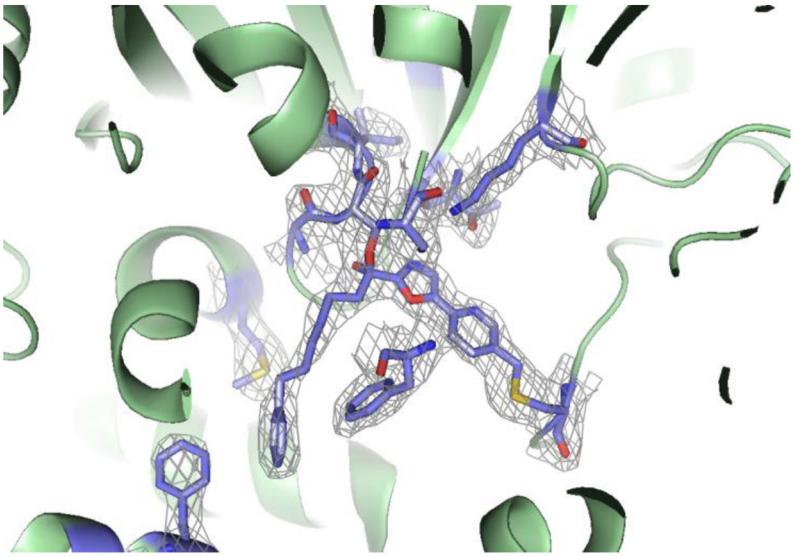

Figure 6.

Inhibitor **3** in the active site of r/hFAAH from the co-crystal structure. The protein backbone is shown as ribbons in green. Select residue side-chains and bound **3** are shown as sticks in light blue (carbon), red (oxygen), blue (nitrogen), and yellow (sulfur). 2Fo-Fc electron density contoured to 1 sigma about the ligand and select side chains is shown as a grey mesh.

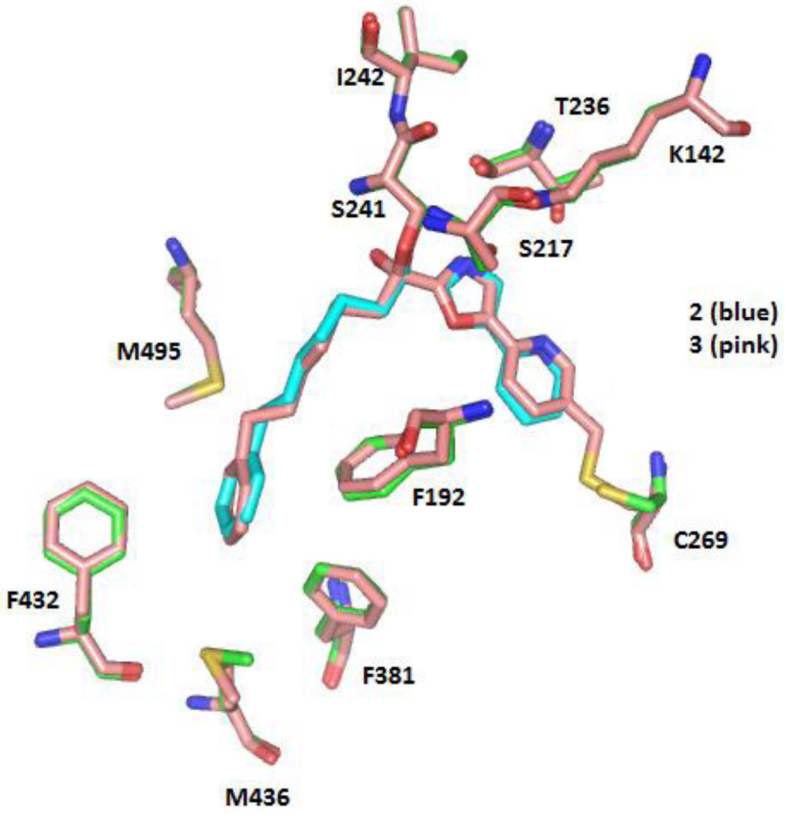

Figure 7.

Overlay of key active site regions of the X-ray co-crystal structures of **3** and **2** bound to r/hFAAH. r/hFAAH residues and bound ligands **2** and **3** are shown as sticks. Carbon atoms corresponding to the co-crystal structure with **2** are shown in green (r/hFAAH) and cyan (**2**) and those corresponding to the co-crystal structure with **3** are shown in pink. Nitrogen, oxygen, and sulfur atoms from both crystal structures are shown in blue, red, and yellow, respectively.

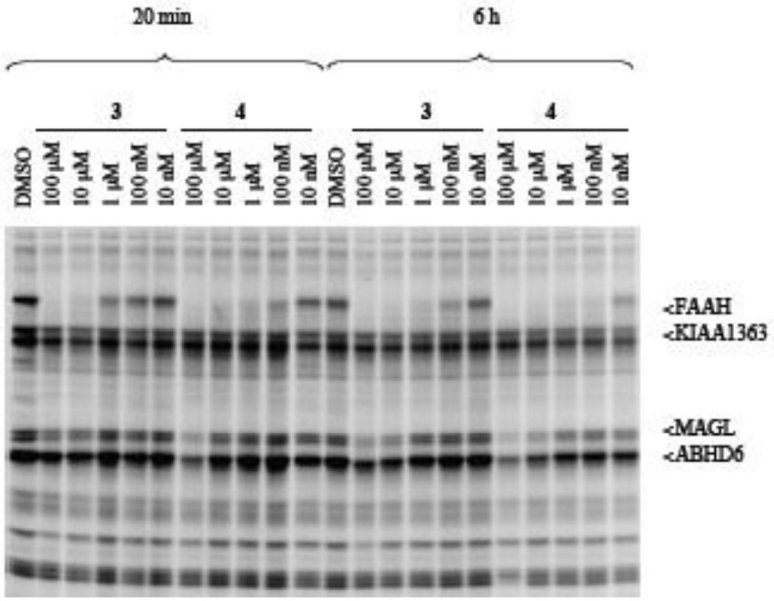

	IC_{50} (nM)			
	20 min		6 h	
enzyme	**3**	**4**	**3**	**4**
FAAH	200	90	30	< 10
KIAA1363	>100,000	>100,000	>100,000	>100,000
TGH	900	450	400	200
MAGL	98,000	50,000	8000	1000
ABHD6	>100,000	97,000	>100,000	95,000

Figure 8.

ABPP screen of **3** and **4** in mouse brain membrane proteome (1 mg/mL) with FP-rhodamine (100 nM). Inhibitor preincubation with the proteome was conducted at both 20 min and 6 h.

AEA Brain, pmol/g (fold increase)

	1 h	3 h	6 h
30 mg/kg	10.7 (2.1)	17.5 (3.5)	18.6 (3.7)
50 mg/kg	13.4 (2.0)	19.0 (3.2)	21.1 (3.5)
Vehicle	6.0	6.0	6.0

OEA Brain, pmol/g (fold increase)

	1 h	3 h	6 h
30 mg/kg	900 (4.5)	1110 (5.3)	1000 (4.7)
50 mg/kg	1040 (5.2)	1100 (5.3)	1100 (5.3)
Vehicle	200	200	200

PEA Brain, pmol/g (fold increase)

	1 h	3 h	6 h
30 mg/kg	1180 (5.8)	2600 (12.3)	2560 (11.6)
50 mg/kg	2510 (12.5)	2940 (13.8)	2900 (13.0)
Vehicle	200	200	200

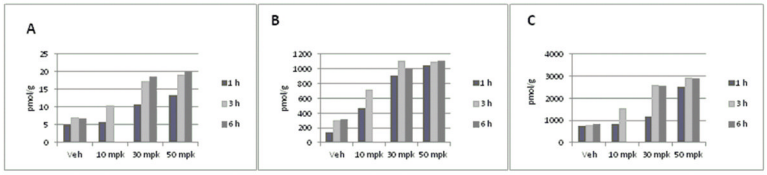

Figure 9.

Lipid levels in the brain 1–6 h post administration of **4**, i.p. at 10, 30, and 50 mg/kg: (A) AEA, (B) OEA, (C) PEA.

AEA Brain, pmol/g (fold increase)			
	1 h	3 h	6 h
2	13.0 (2.2)	9.1 (1.7)	n.d.
4	10.7 (2.1)	19.0 (3.2)	21.1 (3.5)
Vehicle	6.0	6.0	6.0

OEA Brain, pmol/g (fold increase)			
	1 h	3 h	6 h
2	750 (3.7)	300 (1.5)	n.d.
4	900 (4.5)	1100 (5.3)	1000 (4.7)
Vehicle	200	200	200

PEA Brain, pmol/g (fold increase)			
	1 h	3 h	6 h
2	1200 (6.0)	660 (3.3)	n.d.
4	1180 (5.8)	2600 (12.3)	2560 (11.6)
Vehicle	200	200	200

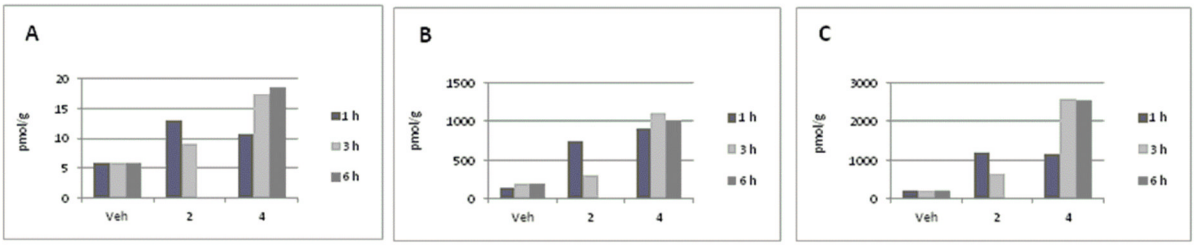

Figure 10.

Comparison of lipid levels in the brain 1–6 h post administration of **2** and **4** at 30 mg/kg, i.p.: (A) AEA, (B) OEA, (C) PEA.

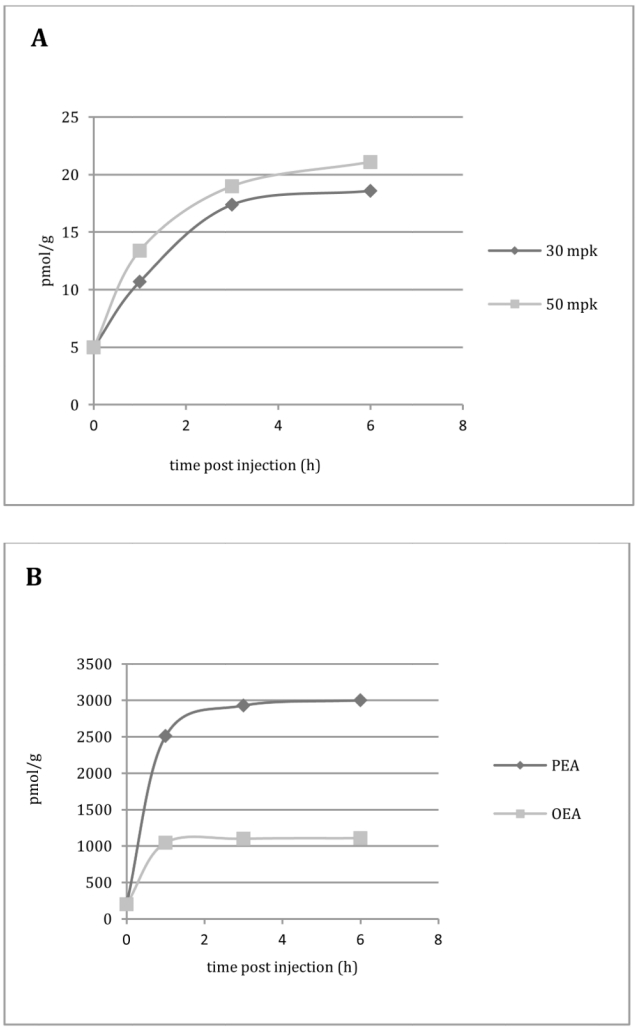

Figure 11.

(A) Levels of anandamide (AEA) in the brain 0–6 h post administration of **4** at 30 and 50 mg/kg administered i.p., and (B) levels of PEA and OEA in the brain 0–6 h post administration of **4** given at 50 mg/kg, i.p.

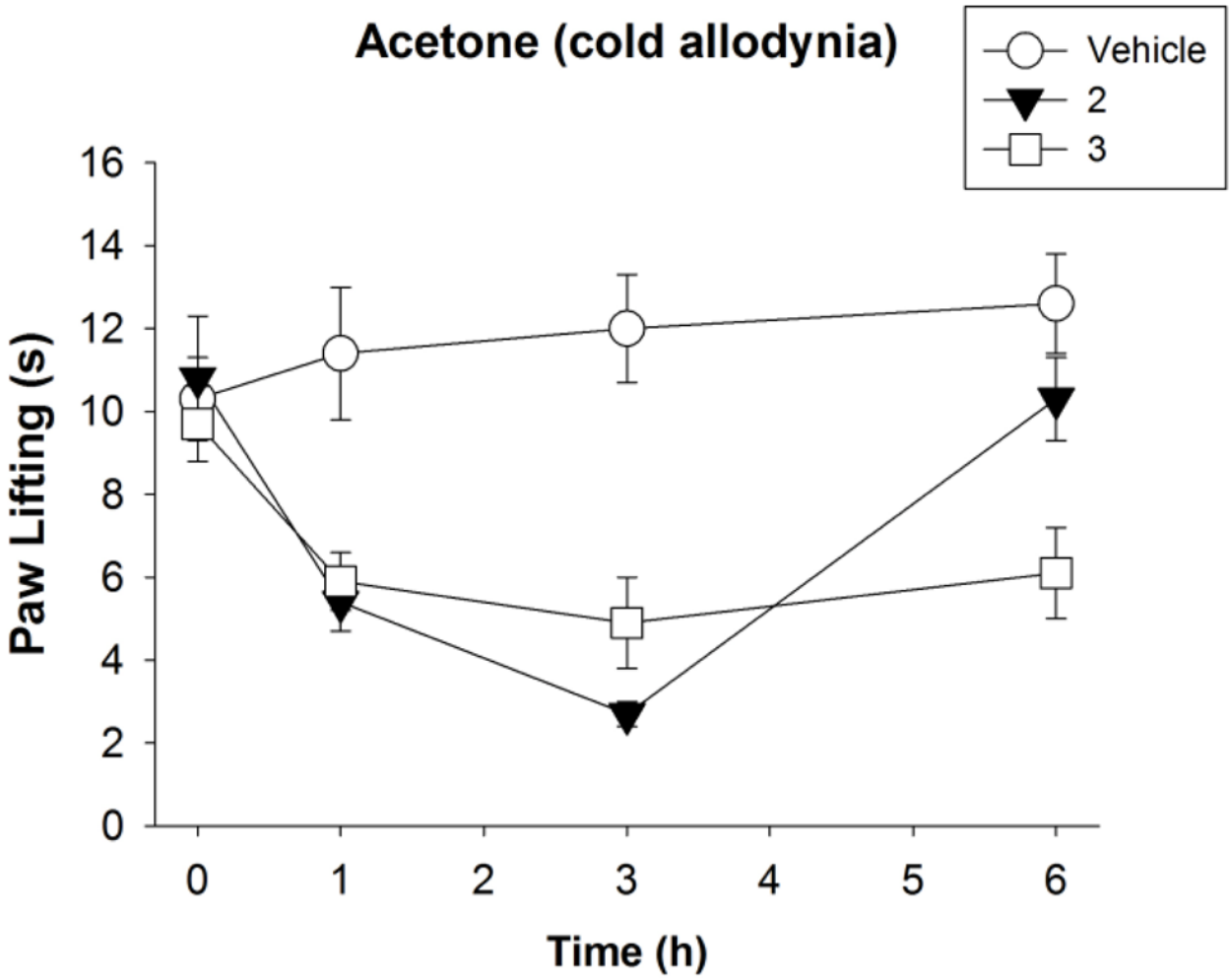

Figure 12.

FAAH inhibition in vivo by **3** significantly attenuated neuropathic pain for >6 h with a potency matching that of the reversible inhibitor **2**, but for a sustained duration. Male C57BL/6 mice were subjected to chronic constriction injury (CCI) of the sciatic nerve and tested 10 days later for mechanical allodynia, as measured with acetone-induced cold allodynia. Inhibitors **2** and **3** (30 mg/kg, i.p.) significantly attenuated CCI-induced cold allodynia in paws ipsilateral to CCI surgery, but had no effect in paws contralateral to CCI surgery. Open circles, vehicle treatment; triangles, **2** treatment; open squares, **3** treatment. Data expressed as mean ± SEM (n = 10).

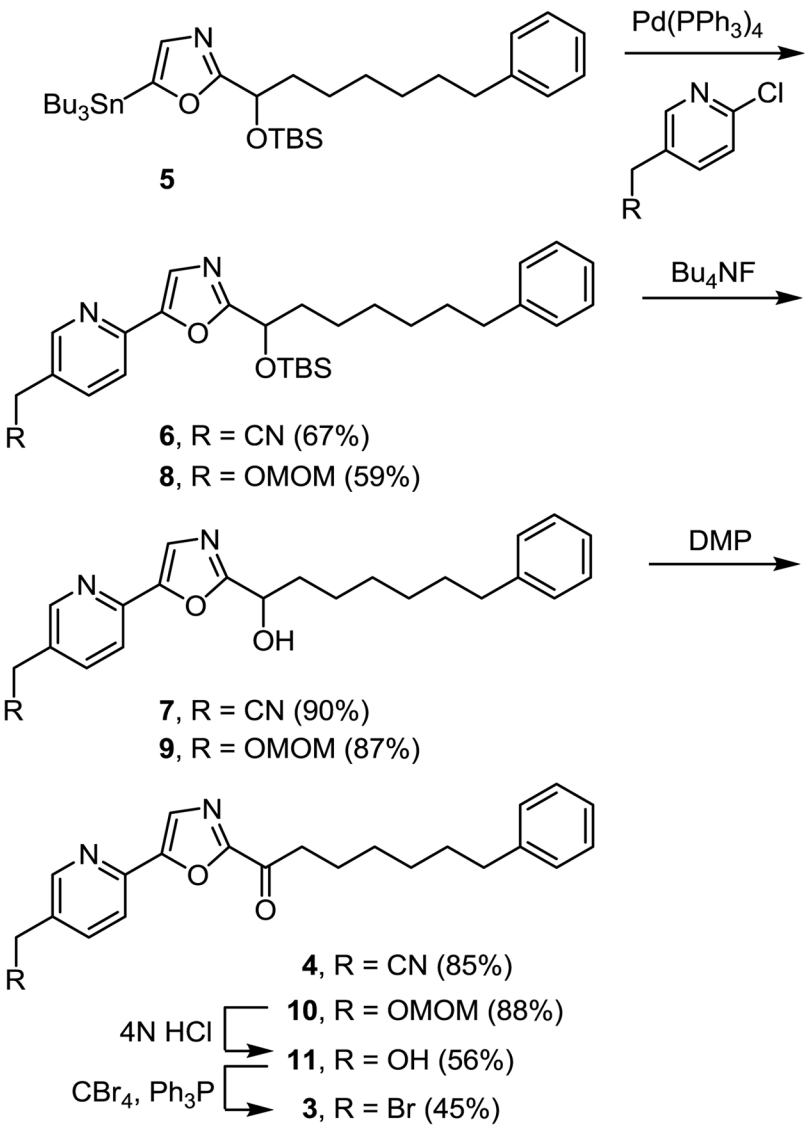

Scheme 1.

Table 1

X-ray Data Collection and Refinement Statistics for r/hFAAH in complex with **3**. Highest resolution shell is shown in parentheses.

	r/hFAAH-3	
Crystal Data		
space group	$P3_221$	
cell dimensions		
a, b, c (Å)	104.1 × 104.1 × 261.0+	
α = β,γ (°)	90, 120	
Data Collection		
processing software	HKL2000	
wavelength (Å)	0.979	
resolution (Å)	50.00 – 2.30	
Rmerge (%)	12.7 (90.9)	
Mean I/σ(I)	11.8 (1.2)	
completeness (%)	97.4 (88.0)	
no. of unique reflections	71, 819	
redundancy	6.4 (2.8)	
Refinement		
resolution (Å)	33.38 – 2.30 (2.36 – 2.30)	
Rwork / Rfree (%)	22.0 / 26.5	
no. of atoms	8,787	
protein	8,405	
ligand	52	
PEG/ion	36	
water	294	
average total B factor (Å^2)	A chain	B chain
protein	61.5	62.2
ligand	66.3	61.4
PEG/ion	69.1	80.2
water	52.4	54.0
Rmsd bond length (Å)	0.016	
Rmsd bond angle (°)	1.764	
Ramachandran plot[a]		
preferred (%)	97.2	
allowed (%)	2.7	
outliers (%)	0.1	

[a] As defined in Molprobity